

## NuSTAR observation of the Vela pulsar and its nebula

OLEG KARGALTSEV,<sup>1</sup> JEREMY HARE,<sup>2,3</sup> AND IGOR VOLKOV<sup>1</sup>

<sup>1</sup>*Department of Physics, The George Washington University, 725 21st St. NW, Washington, DC 20052*

<sup>2</sup>*NASA Goddard Space Flight Center, Greenbelt, MD, 20771*

<sup>3</sup>*NASA Postdoctoral Program Fellow*

### ABSTRACT

We present the analysis of 200-ks NuSTAR observation of the Vela pulsar and PWN. The phase-resolved spectra corresponding to two main peaks in the folded pulse profile differ significantly. The spectrum of Peak 1 is significantly harder than that of Peak 2 in qualitative agreement with the earlier RXTE results. However, for both spectra, the values of power-law (PL) fit photon indices,  $\Gamma$ , are noticeably larger than the previously reported values. The hardest (Peak 1) spectrum has  $\Gamma = 1.10 \pm 15$  which is close to those of the bright inner PWN jets. We used the off-pulse interval to isolate pulsar emission from the compact pulsar wind nebula (PWN) emission. We also measured the spectrum from the south-western (SW) region of the PWN which is resolved by NuSTAR from the compact PWN. For both regions we fitted the NuSTAR spectra by themselves and together with the CXO spectra (extracted from the same regions). We found that the compact PWN spectrum requires a more complex model than a simple PL but we did not find evidence for strong cooling, such as an exponential cutoff (particularly, for the more remote SW region). These results imply energies of  $\gtrsim 600$  TeV for the X-ray emitting particles and place some constraints on the particle transport within the PWN.

### 1. INTRODUCTION

Vela pulsar (PSR B0833-45), the youngest of the few nearby pulsars, has been extensively studied across the electromagnetic spectrum (see e.g., (Romani et al. 2005)). It is the brightest GeV gamma-ray pulsar. Pulsar's spectrum is non-thermal everywhere but in soft X-rays where thermal emission from the neutron star (NS) surface dominates (Pavlov et al. 2001). Outside the soft X-ray range (Sanwal et al. 2002) the phase-integrated multiwavelength spectrum shows complex behavior implying multiple breaks (e.g., Danilenko et al. 2011). The multiwavelength lightcurves are similarly complex with up to 6 discernible peaks during the 89-ms pulse period (see Figure 5 of Spolon et al. 2019). The peaks relative strengths vary with energy. These changes are noticeable even across the relatively narrow, 2–30 keV, range explored with RXTE (Harding et al. 2002; Kuiper & Hermsen 2015). By performing phase-resolved analysis of RXTE data Harding et al. (2002) also found that the peak's spectra can be described by a power-law with photon indices,  $\Gamma$  ranging from 0.8 to 2.1. The lowest value of  $\Gamma$  indicates a very hard spectrum that is hardly compatible with the synchrotron emission and is also harder than the spectrum of the hardest part of the pulsar wind nebula (PWN),  $\Gamma \approx 1.2$  (Kargaltsev & Pavlov 2004; Kargaltsev et al. 2017).

Thanks to the young age ( $\approx 11$  kyrs) and relatively high spin-down power ( $\dot{E} = 7 \times 10^{36}$  erg s<sup>-1</sup>) the pulsar inflates a bubble filled with the pulsar wind (PWN) within the Vela SNR interior (Bock et al. 1998; Dodson et al. 2003). The compact axisymmetric PWN exhibits a complex fine structure (both spatial and spectral) resolved in the Chandra X-ray Observatory (CXO) images (Pavlov et al. 2001; Helfand et al. 2001; Pavlov et al. 2003; Durant et al. 2013), thanks to the proximity of the pulsar located at  $d = 350$  pc. Spectral maps of the compact PWN (Kargaltsev et al. 2017) indicate that the Vela PWN has one of the hardest X-ray spectra among all known PWNe. On larger scales the PWN is asymmetric, extending much further away from the pulsar in the SW direction compared to the NE side. The spatially-resolved spectroscopy of the Vela PWN has been limited to CXO ACIS data which cover 0.5–8 keV range in photon energies.

We obtained NuSTAR observation of the Vela PWN to extend the spectral coverage out to 70 keV, resolving the large-scale PWN, measure the properties of the pulsed emission while also separating pulsar emission from that of the PWN using photon phases. In Section 2 we describe the data used in this paper, Section 3 and 4 report the results of timing and spectral analysis, respectively. The discussion of our results is provided in Section 5. We conclude with the summary in Section 6.

## 2. OBSERVATIONS

### 2.1. NuStar

*NuSTAR* (Harrison et al. 2013) observed the Vela pulsar region on 2021 March 21 ((ObsIDs 30601032002; start time MJD 59294.66333575769) for the total duration of 205,271 s. We reprocessed the data using HEASoft v6.28 and *NuSTAR* CALDB v20210427. We ran the standard `nupipeline` tool, which applied all the latest calibrations and filtering, and barycenter-corrected the arrival times of photons originating from the pulsar’s position, using *NuSTAR* clock correction file 20100101v119 which also corrects for *NuSTAR*’s clock drift, providing a timing accuracy of  $\sim 65 \mu\text{s}$  (Bachetti et al. 2021). We excluded times of high particle background using the options `saacalc=2`, `saemode=optimized`, and `tentacle=no`, which had a minimal impact on the total exposure time (i.e.,  $< 0.2\%$ ). We extracted spectra using `nuproducts` (with option `extended=yes` for analysis of the PWN).

### 2.2. Chandra X-ray Observatory

We used archival CXO ACIS data (from 3 observations obtained between Aug 15 2010 and Sep 4 2010; ObsIDs 12073, 12074, and 12075; total exposure 121 ks) to improve the statistics and extend the energy range of *NuStar* data. The data reduction and fits followed standard procedures described in CIAO threads. For our analysis we used CIAO CIAO 4.13 and CALDB 4.9.4.

## 3. TIMING

To produce *NuSTAR* pulse profiles we performed  $Z_n^2$  test (for  $n=5$ , given the multi-peak nature of the hard X-ray pulse profile; Harding et al. 2002) on a 2D grid of frequency ( $f$ ) and frequency derivative ( $\dot{f}$ ). We also vary the circular extraction aperture radius, to maximize the pulsar contribution, and found that the  $Z_5^2$  values grow up to  $r = 50''$  (which includes 349,527 photons of which most are due to PWN) and then levels off. Finally, we explored the dependence of  $Z_5^2$  on the energy range and found that it is maximized if the full range (3–79 keV) is used. The results of these experiments are shown in Tables 1 and 2 and Figure 1. The latter also shows the frequency and frequency derivative predicted based on the Fermi LAT ephemeris based on 13.2 years of LAT data and having the validity range MJD 54682.71577–59500.98129. The agreement shows that the *NuSTAR* timing is accurate. Comparison between LAT and *NuSTAR* profiles in Figure 2 shows that at least 3 peaks seen in *NuStar* data have counterparts in Fermi LAT pulse profile, including the two main peaks dubbed Peak 1 (Pk1) and Peak 2 (Pk2).

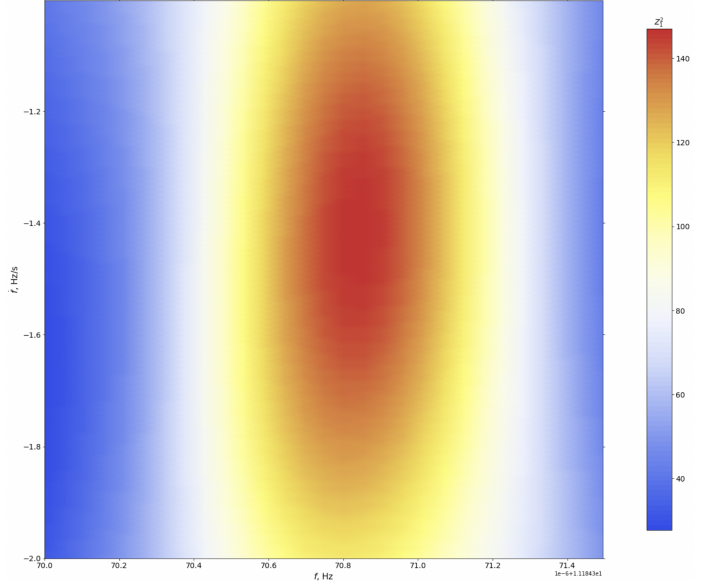


**Figure 1.**  $Z_5^2$  distribution as a function of frequency and its derivative for *NuStar* data.

Next, we assigned all photons detected in *NuSTAR* observation the value of pulsar phase using the `....` task from `ftools` with  $f = 11.184370843830187 \text{ Hz}$  and  $\dot{f} = -1.5889658245931358 \times 10^{-11} \text{ s s}^{-1}$  at MJD 59296.8303. The folded pulse profile in 3–79 keV is shown in Figure 2 (top) together with the folded LAT pulse profile (Figure 2; bottom). We also show the phase ranges corresponding to main peak and to the secondary peak in the  $\gamma$ -ray pulse profile.

## 4. SPECTRA

### 4.1. Pulsar

Since the PWN photons strongly dominate pulsar photons within the chosen  $50''$  aperture, we only fit pulsar spectrum in two phase bins corresponding to the main and secondary peaks in the  $\gamma$ -ray pulse profile. Since the intervening hydrogen column is small (see, e.g., ), we simply fitted a power-law model to the the Peak 1 ( $\phi = 0.06 – 0.22$ ) and Peak 2 ( $\phi = 0.70 – 0.78$ ) spectra using the spectrum from the Off-Pulse interval spectrum ( $\phi = 0.28 – 0.34$ ) as a background. The Peak 1 spectrum with  $\Gamma_1 = 1.10 \pm 0.15$  is substantially harder than Peak 2 spectrum with  $\Gamma_2 = 1.62 \pm 0.20$ . The PL fit quality is good for both Peak 1 and 2 spectra.

### 4.2. PWN

In order to explore the PWN spectrum we define two regions, one for compact PWN and one for the SE extension (white and green in Figure 4, respectively). For the compact PWN region we used both all and only off-pulse events to avoid contamination by the pulsar (although it

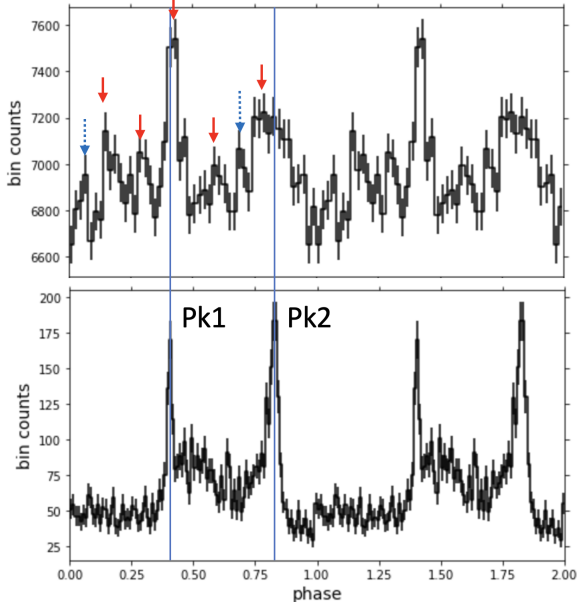


**Figure 2.** The top panel shows NuSTAR 3-79 pulse profile of Vela pulsar (with 20 phase bins) folded with Fermi LAT ephemeris. The red solid arrows show peaks clearly discernible in the RXTE 4-8 keV pulse profile from Figure 4 of (Kuiper & Hermsen 2015). The bottom panel shows Fermi LAT pulse profile in 0.3-6 GeV band produced from the same time interval as that covered by NuSTAR observation.

contribution is small, only about 4%-5% of total counts in 3-8 keV). We first fit NuStar only spectra<sup>1</sup> (in 3-79 keV range) and then perform joint fits by adding archival CXO data. In all fits the normalizations of different detectors (FPMA, FPMB, and ACIS) are allowed to vary independently while the rest of fitting parameters are tied.

For the compact PWN we first performed the fit in the wider off-pulse region ( $\Delta\phi = 0.06$ ) which contains 9,661 (FPMA) and 10,557 (FPMB) photons in 3-79 keV (99% of counts come from the source meaning not the diffuse background) and excludes any detectable contribution of the *pulsed* pulsar component. We group the spectrum by 200 photons per bin prior to fitting with PL model. The best-fit  $\Gamma = 1.64 \pm 0.01$  but fit quality is not great with  $\chi^2 = 141.01$  for 91 d.o.f. and some systematic large-scale residuals at low and high energies of the energy range used for the fit. We, therefore, tried to also fit a broken PL model (“bknpower” in XSPEC) and obtained  $\Gamma_1 = 1.57 \pm 0.02$ , break energy  $E_b = 10.9 \pm 1.5$  and  $\Gamma_2 = 1.79 \pm 0.05$  with a noticeable improvement in large-scale residuals with  $\chi^2 = 127.63$  for 89 d.o.f. We

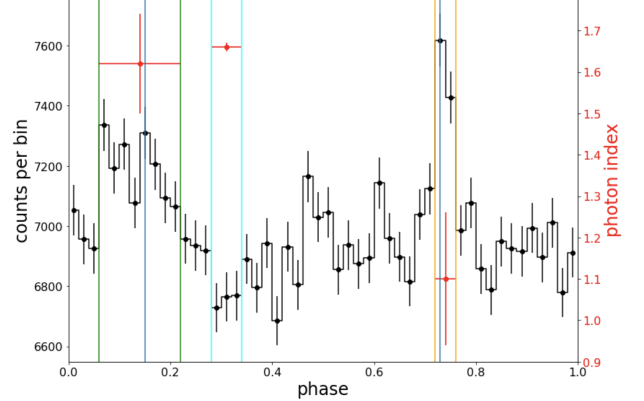


**Figure 3.** NuSTAR 3-79 pulse profile of Vela. The red shows the main peak, green shows the secondary peak, and the black shows the lowest flux bin, which we use to model the background contribution due to the bright PWN.

next fitted the spectrum from the same region without filtering on pulsar phase given that the pulsar’s pulsed contribution is small. The statistics is now much better with 182,237 in FPMA and 166,675 photons in FPMB of which 99% come from the source (meaning not diffuse background) in either of the detectors. We group the spectrum requiring 500 counts per bin. With the same broken PL model we obtain values which are very close to the above fit:  $\Gamma_1 = 1.58 \pm 0.01$ , break energy  $E_b = 8.9 \pm 0.4$  and  $\Gamma_2 = 1.72 \pm 0.01$ . The quality of the fit is good:  $\chi^2 = 516.65$  for 491 d.o.f. The very small differences to the off-pulse interval spectrum suggest the pulsar indeed does not noticeable affect the spectral fit for PWN in 3-79 keV. The single PL fit gives best fit  $\Gamma = 1.65$  but its quality not satisfactory ( $\chi^2 = 701.34$  for 493 d.o.f.) with prominent large-scale residuals similar in shape to those seen for the off-pulse phase interval spectrum. Finally, taking advantage of a excellent statistics and no noticeable impact from the pulsar, we also tried to fit a PL with exponential cutoff. Although the quality of the fit ( $\Gamma = 1.56 \pm 0.01$  and  $E_c = 121^{+11}_{-10}$  keV) is acceptable ( $\chi^2 = 552.05$  for 492 d.o.f.), it is worth than for the broken PL and large-scale residuals are becoming noticeable. Therefore, a broken PL description is statistically preferred.

For the SW extension region spectrum bined to at least 100 per bin and having 17,059 and 16,380 photons in FPMA and FPMB, respectively, (with 80% coming from the source for either of the detectors) the PL fit gives  $\Gamma = 1.808 \pm 0.015$  with  $\chi^2 = 281.57$  for 258 d.o.f. There are no noticeable systematic residuals. Therefore, we have not attempted any more complex fits.

We now describe the joint fits with NuStar and CXO ACIS. In all of these fits we used models modified by ISM absorption modeled with XSPEC’s “tbabs” with

<sup>1</sup> The photon indices are tied for fpmA and fpmB but normalizations are free

$n_H = 3.2 \times 10^{20} \text{ cm}^{-2}$ . For the SW extension PWN region with jointly fit spectra in 1-79 keV range. The single PL fit is bad with strong large-scale residuals. Both broken PL and PL with exponential cutoff models are providing good fits. For the former,  $\Gamma_1 = 1.61 \pm 0.02$ , break energy  $E_b = 3.0 \pm 0.3$  and  $\Gamma_2 = 1.81 \pm 0.01$ . The low energy of the break explains why the broken PL model was not required when only NuStar data were fitted within 3-79 keV range. On the other hand, the coincidence between the  $E_b$  and the start of NuStar energy range may indicate that the need for the broken PL comes from imperfection in calibration and simply reflect the insufficient quality of cross-calibration (see also Madsen et al. 2017). The best-fit models are shown in Figure 5. If so, we could expect a similar situation with the fits for the compact PWN region. For these regions, we jointly fit spectra in 0.8-79 keV range (since there are plenty of photons in ACIS even at low energies where the detector is insensitive). All spectra are binned to have at least 200 counts per bin. The ACIS spectrum has 718,271 photons. We exclude the  $r = 3''$  region centered on the pulsar in the CXO ACIS data and we use the off-pulse phase interval for NuStar data in order to completely exclude the pulsar. We also excluded a narrow region near 2 keV in the CXO data because it seems to show local residuals which could be instrumental. Not surprisingly the simple absorbed PL fit is not satisfactory. Even the broken PL fit is not great ( $\chi^2 = 544.85$  for 473 d.o.f.) with systematic negative (model overpredicting data) residuals appearing above 20 keV. The best-fit parameters are  $\Gamma_1 = 1.450 \pm 0.048$ , break energy  $E_b = 2.7 \pm 0.1$  and  $\Gamma_2 = 1.60 \pm 0.01$ . The break energy is again close to the lower energy of NuStar range hinting at a possible calibration issue. On the other hand, such behavior is not surprising because the spectrum is expected to change (soften) gradually with the distance from the pulsar (REF) and, therefore, a PL with a single break can only be an approximation. The fit with exponentially cutoff PL is not statistically better compared to the broken PL.

## 5. DISCUSSION

### 5.1. Pulsar

NuSTAR pulse profile of Vela pulsar is remarkably complex in 3-79 keV range with multiple narrow peaks of which two align well with those seen in the LAT pulse profile (see Figure 2). Overall the NuSTAR pulse profile looks very similar to the one obtained from RXTE data dating back more than two decades. In particular, all 5 peaks (two main peaks Pk1 and Pk2 and 3 smaller ones) are easily identifiable in both NuSTAR and RXTE pulse profiles (see Figure 4 of Kuiper & Hermsen (2015)).

**Table 1.** Maximum values of  $Z_5^2(f, \dot{f})$  for different energy ranges using a  $50''$  aperture.

Energies	$N$	$f$	$\dot{f}$	$Z_5^2$
keV	counts	Hz	$10^{-11} \text{ Hz/s}$	
1.6-40	366279	11.18437085	-1.40	133.757
3-40	345449	11.18437085	-1.41	133.878
3-50	347627	11.18437085	-1.41	138.458
3-60	348659	11.18437085	-1.42	139.504
3-70	349213	11.18437085	-1.42	141.407
3-79	349527	11.18437085	-1.42	142.375

**Table 2.** Maximum values of  $Z_5^2(f, \dot{f})$  for different aperture sizes in the 3-79 keV energy range.

Aperture $r$	$N$	$f$	$\dot{f}$	$Z_5^2$
arcsec	counts	Hz	$10^{-11} \text{ Hz/s}$	
5	8250	11.18437128	-1.70	21.291
10	33483	11.18437085	-1.00	41.910
20	110926	11.18437091	-1.33	63.370
30	199966	11.18437085	-1.52	86.308
40	280952	11.18437085	-1.45	122.806
50	349527	11.18437085	-1.42	142.375
60	405356	11.18437085	-1.46	141.019
70	451124	11.18437085	-1.44	152.912
80	488106	11.18437085	-1.49	149.750
90	519326	11.18437085	-1.48	152.607
100	545400	11.18437080	-1.49	147.114

**Table 3.** Phase-resolved spectral fitting results.

Feature name	Phase range	$\Gamma$
Narrow peak small (Pk1)	0.72-0.76	$1.10 \pm 0.15$
Broad peak (Pk2)	0.06-0.22	$1.62 \pm 0.20$
Background	0.28-0.34	$1.52 \pm 0.01$

This means that the pulse profile remains stable despite the prolific glitching activity that Vela exhibits. NuSTAR profile suggests two additional peaks that have no counterparts in the RXTE pulse profiles but these small peaks could be due to the noise fluctuations.

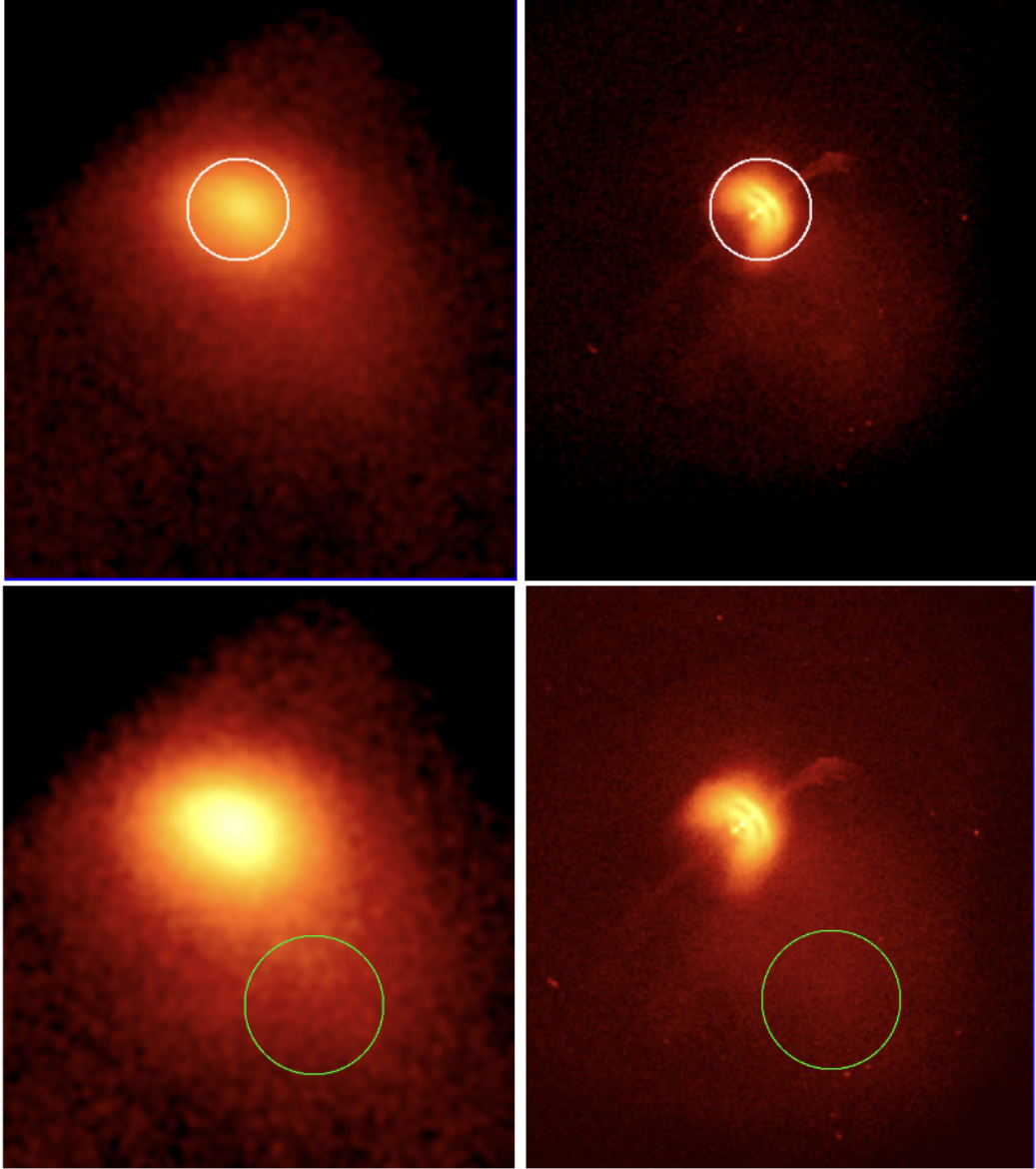


**Figure 4.** *NuSTAR* 3-79 keV (left) and *CXO* (right) images of the Vela PWN showing the same region of the sky. The white ( $r = 50''$ ) and green ( $r = 1.2'$ ) circles show spectral extraction regions from the compact PWN and SW extension region, respectively. North is up, East is to the left.

Due to the coarse resolution, the pulsar is not resolved well from the surrounding bright compact PWN. Therefore, pulsed component makes only a small contribution on top of PWN emission in the pulse profile. This only allows us to extract meaningful spectra for 2 main peaks by taking photons from the pulse minimum interval as the background. Although the Peak 1 spectrum ( $\Gamma_1 = 1.10 \pm 0.15$ ) is substantially harder than Peak 2 spectrum ( $\Gamma_2 = 1.62 \pm 0.20$ ), in qualitative agreement with (Harding et al. 2002), the actual best fit values are different significantly larger than those reported by Harding et al. (2002) ( $\Gamma_{1,\text{RXTE}} = 0.68 \pm 0.14$  and  $\Gamma_{2,\text{RXTE}} = 1.17 \pm 0.12$ ). We attribute the differ-

ences to a different choice of background in the RXTE data analysis.

The new, larger values, are comparable to the photon index values for the hardest elements of the compact bright PWN (see Kargaltsev et al. 2017).

## 5.2. PWN

Thank to the faintness of the pulsar above 3 keV it makes negligible impact onto PWN spectrum as we show by fitting the spectrum from the entire PWN region for all phases and then the spectrum for the same region but with phases restricted to the pulse minimum interval. The differences are negligible. By fitting just NuS-

TAR spectrum and by jointly fitting NuStar and CXO ACIS spectra we find that a single PL cannot describe the spectrum of the compact PWN extracted from an  $r = 50''$  circle centered on the pulsar. At least one spectral break is required to describe the softening of the spectrum with energy. This shows that cooling makes substantial impact onto the compact PWN spectrum in agreement with what was observed for this region in the high-resolution CXO spectral maps restricted to a much narrow energy range. The noticeable cooling during the particle residence time (dynamic timescale) must be attributed to the sufficiently strong magnetic field within the compact PWN.

The maximum energy available for particle acceleration,  $E_{\max} = e(\dot{E}/c)^{1/2} = 4.6$  PeV, which corresponds to electron Lorentz factor  $\gamma_{\max} = 9 \times 10^9$ . Using standard synchrotron theory (Kargaltsev et al. 2002) provided an estimate of magnetic field in Vela PWN which gives  $B \approx 50 \mu\text{G}$  for the compact PWM and  $B \approx 30 \mu\text{G}$  for the SW region. For these values of magnetic field observing synchrotron photons with energies of 70 keV implies electron energies of  $\gamma \sim 3.6 \times 10^8 (E_{\text{syn}}/70 \text{ keV})^{1/2} (B/30 \mu\text{G})^{-1/2}$  which is about 4% of the potential drop available in the pulsar magnetosphere (for dipolar geometry). The corresponding synchrotron cooling time can be estimated as  $\tau_c \approx 10(B/30 \mu\text{G})^{-3/2} (E/70 \text{ keV})^{-1/2}$  yrs.

We note that the  $\Gamma \approx 1.8$  that we find above  $E_b = 10$  keV for the broken PL fit to the NuStar spectrum of the compact PWN and PL fit to the SW region spectrum are consistent with the OSSE result,  $\Gamma = 1.8 \pm 0.4$  in 44–760 KeV, reported by de Jager et al. (1996). On the other hand, (Mattana et al. 2011) reported a slightly softer spectrum with  $\Gamma = 2.00 \pm 0.04$  in from INTEGRAL IBIS/ISGRI data in 18–400 keV. The slightly softer spectrum probably reflects the fact that there is additional cooling within the larger region ( $r = 6'$ ) used for the extraction of the IBIS/ISGRI data. In any case, there appears to be solid evidence for spectral cut-off up to at least few hundred keV which implies that the electrons are accelerated to at least 10% of the energy available from the potential drop. The 100% efficiency would be achieved for synchrotron photons with energy of about 60 MeV. Sensitive observations in MeV range are needed to establish the maximum energy of the electron SED. Comparison with results reported from high-resolution spectral maps (Kargaltsev et al. 2017) shows that the PWN spectrum softens from  $\Gamma \approx 1.3$  to  $\Gamma \approx 1.8$  over the

distance of  $\approx 3'$  corresponding to  $\approx 0.26$  pc at  $d = 300$  pc. The fairly mild cooling and the existence of particles emitting 70-keV photons at  $\approx 0.26$  pc from the pulsar implies fairly fast particle transport. If it can be described by a bulk plot then the average flow speed would be about  $0.08c$ . Alternatively, it is possible that at these distances particles are mostly transported by diffusion, in which case the corresponding timescale is given by  $\tau_d = \bar{l}^2/2D_B = 26(\gamma/4 \times 10^8)^{-1} (B/30 \mu\text{G})(\bar{l}/0.26 \text{ pc})^2$  where Bohm diffusion coefficient,  $D_B$ , was assumed (see e.g., Porth et al. 2016). Therefore if the transport occurring primarily in diffusive manner then the diffusion cannot be much slower than Bohm diffusion. Alternatively, the slow cooling could be attributed to the in-situ particle acceleration which may be caused by magnetic turbulence (Xu et al. 2019).

## 6. SUMMARY AND CONCLUSION

NuStar data support a very complex structure of pulse profile in 3–79 keV with 5–7 Peaks per period. By isolating photons with phases belonging to two main peaks (Peak 1 and 2) in the pulse profile we extracted the phase-resolved spectra and fitted them with PL model finding photon indices of  $1.10 \pm 0.15$  and  $1.62 \pm 0.20$ , respectively. These values are substantially larger than those found earlier from RXTE data.

The fit to NuSTAR and CXO+NuSTAR spectrum for the compact PWN requires more complex model than simple PL and can be empirically described by a broken PL. The observed softening is likely attributed to mild synchrotron cooling. The presence of particles emitting  $\sim 70$ -keV synchrotron photons about  $3'$  away from the pulsar implies rather fast transport. The observed mild cooling with the distance requires either bulk flow with average flow speed of  $0.08c$ , rapid diffusion, or in-situ acceleration. The observed energies of synchrotron photons imply that at least 4% (or, 10%, accounting for previous observations at higher energies) of the polar cap potential drop is used to accelerate pulsar wind particles.

## Acknowledgments:

Support for this work was provided by the National Aeronautics and Space Administration through the NuSTAR award 80NSSC21K0024. JH acknowledges support from an appointment to the NASA Postdoctoral Program at the Goddard Space Flight Center, administered by the Universities Space Research Association under contract with NASA.

## REFERENCES

- Romani, R. W., Kargaltsev, O., & Pavlov, G. G. 2005,  
ApJ, 627, 383.  
doi:10.1086/43026910.48550/arXiv.astro-ph/0503331

- Danilenko, A. A., Zyuzin, D. A., Shibanov, Y. A., et al.  
2011, MNRAS, 415, 867. doi:10.1111/j.1365-  
2966.2011.18753.x10.48550/arXiv.1103.4871

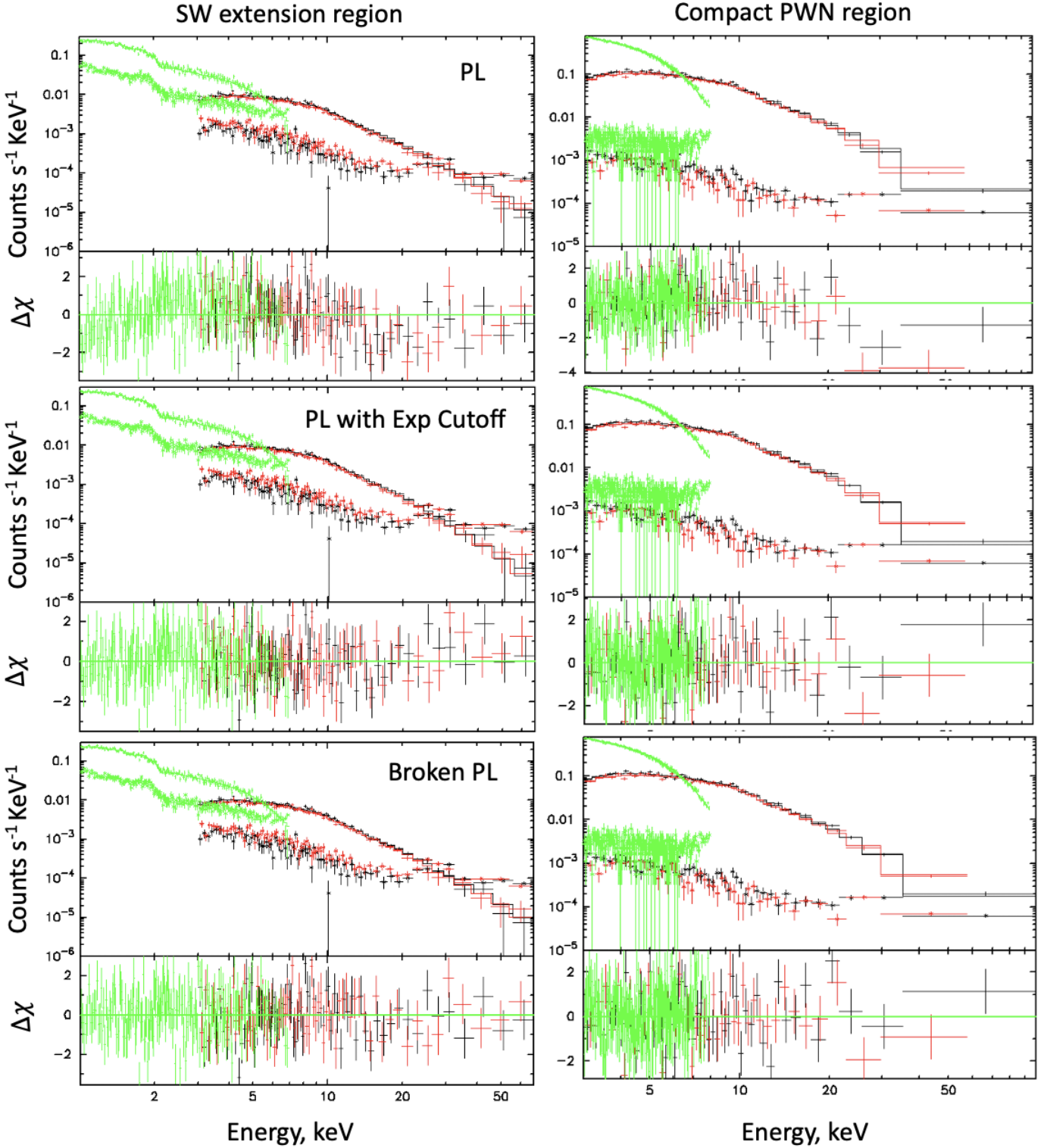


**Figure 5.** Joint fits to NuStar (black and red; for FPMA and FPMB, respectively) and CXO (green) spectra. Background contribution is also shown for each detector/instrument.

- Harding, A. K., Strickman, M. S., Gwinn, C., et al. 2002, *ApJ*, 576, 376.  
doi:10.1086/34173210.48550/arXiv.astro-ph/0205183
- Pavlov, G. G., Zavlin, V. E., Sanwal, D., et al. 2001, *ApJL*, 552, L129.  
doi:10.1086/32034210.48550/arXiv.astro-ph/0103171
- Spolon, A., Zampieri, L., Burtovoi, A., et al. 2019, *MNRAS*, 482, 175.  
doi:10.1093/mnras/sty260510.48550/arXiv.1809.07093
- Kargaltsev, O. & Pavlov, G. 2004, Young Neutron Stars and Their Environments, 218, 195.  
doi:10.48550/arXiv.astro-ph/0310767
- Kargaltsev, O., Klingler, N., Chastain, S., et al. 2017, *Journal of Physics Conference Series*, 932, 012050.  
doi:10.1088/1742-6596/932/1/012050
- Pavlov, G. G., Kargaltsev, O. Y., Sanwal, D., et al. 2001, *ApJL*, 554, L189.  
doi:10.1086/32172110.48550/arXiv.astro-ph/0104264
- Helfand, D. J., Gotthelf, E. V., & Halpern, J. P. 2001, *ApJ*, 556, 380.  
doi:10.1086/32153310.48550/arXiv.astro-ph/0007310
- Sanwal, D., Pavlov, G. G., Kargaltsev, O. Y., et al. 2002, *Neutron Stars in Supernova Remnants*, 271, 353.  
doi:10.48550/arXiv.astro-ph/0112164
- Durant, M., Kargaltsev, O., Pavlov, G. G., et al. 2013, *ApJ*, 763, 72. doi:10.1088/0004-637X/763/2/7210.48550/arXiv.1211.0347
- Pavlov, G. G., Teter, M. A., Kargaltsev, O., et al. 2003, *ApJ*, 591, 1157.  
doi:10.1086/37553110.48550/arXiv.astro-ph/0305510
- Dodson, R., Lewis, D., McConnell, D., et al. 2003, *MNRAS*, 343, 116. doi:10.1046/j.1365-8711.2003.06653.x10.48550/arXiv.astro-ph/0302373
- Bock, D. C.-J., Turtle, A. J., & Green, A. J. 1998, *AJ*, 116, 1886.  
doi:10.1086/30056310.48550/arXiv.astro-ph/9807125
- Harrison, F. A., Craig, W. W., Christensen, F. E., et al. 2013, *ApJ*, 770, 103. doi:10.1088/0004-637X/770/2/10310.48550/arXiv.1301.7307
- Madsen, K. K., Forster, K., Grefenstette, B., et al. 2022, *Journal of Astronomical Telescopes, Instruments, and Systems*, 8, 034003.  
doi:10.1117/1.JATIS.8.3.03400310.48550/arXiv.2110.11522
- Bachetti, M., Markwardt, C. B., Grefenstette, B. W., et al. 2021, *ApJ*, 908, 184. doi:10.3847/1538-4357/abd1d610.48550/arXiv.2009.10347
- Kuiper, L. & Hermsen, W. 2015, *MNRAS*, 449, 3827.  
doi:10.1093/mnras/stv426
- Kargaltsev, O., Pavlov, G. G., Sanwal, D., et al. 2002, *Neutron Stars in Supernova Remnants*, 271, 181
- de Jager, O. C., Harding, A. K., & Strickman, M. S. 1996, *ApJ*, 460, 729. doi:10.1086/177005
- Mattana, F., Götz, D., Terrier, R., et al. 2011, *ApJL*, 743, L18. doi:10.1088/2041-8205/743/1/L18
- Porth, O., Vorster, M. J., Lyutikov, M., et al. 2016, *MNRAS*, 460, 4135. doi:10.1093/mnras/stw1152
- Xu, S., Klingler, N., Kargaltsev, O., et al. 2019, *ApJ*, 872, 10. doi:10.3847/1538-4357/aafb2e
- Madsen, K. K., Forster, K., Grefenstette, B., et al. 2022, *Journal of Astronomical Telescopes, Instruments, and Systems*, 8, 034003. doi:10.1117/1.JATIS.8.3.034003
- Madsen, K. K., Beardmore, A. P., Forster, K., et al. 2017, *AJ*, 153, 2. doi:10.3847/1538-3881/153/1/2